Journal of Power Sources 195 (2010) 1691–1697

Contents lists available at ScienceDirect

Journal of Power Sources

journal homepage: www.elsevier.com/locate/jpowsour

Vapor-induced solid–liquid–solid process for silicon-based nanowire growth

Ji-Guang Zhang[a,*], Jun Liu[a], Donghai Wang[a], Daiwon Choi[a], Leonard S. Fifield[a], Chongmin Wang[a], Gordon Xia[a], Zimin Nie[a], Zhenguo Yang[a], Larry R. Pederson[b], Gordon Graff[a]

[a] Pacific Northwest National Laboratory, Richland, WA 99354, United States
[b] North Dakota State University, Fargo, ND 58102, United States

ARTICLE INFO

Article history:
Received 5 August 2009
Received in revised form
28 September 2009
Accepted 30 September 2009
Available online 12 October 2009

Keywords:
Lithium ion batteries
Silicon
Nanowire
Energy storage
SiC
PHEV

ABSTRACT

Silicon-based nanowires have been grown from commercial silicon powders under conditions with different oxygen and carbon activities. Nanowires grown in the presence of carbon sources consisted of a crystalline SiC core with an amorphous SiO_x shell. The thickness of the SiO_x shell decreased as the oxygen concentration in the precursor gases decreased. Nanowires grown in a carbon-free environment consisted of amorphous silicon oxide with a typical composition of $SiO_{1.8}$. The growth rate of nanowires decreased with decreasing oxygen content in the precursor gases. $SiO_{1.8}$ nanowires exhibited an initial discharge capacity of ~1300 mAh g^{-1} and better stability than those of silicon powders. A vapor-induced solid–liquid–solid (VI-SLS) mechanism is proposed to explain the nanowire growth (including silicon and other metal-based nanowires) from powder sources. In this approach, both a gas source and a solid-powder source are required for nanowire growth. This mechanism is consistent with experimental observations and also can be used to guide the design and growth of other nanowires.

Published by Elsevier B.V.

1. Introduction

Energy-storage technologies, particularly lithium-ion batteries, have been a focal point for the development of advanced, fuel-efficient vehicles, especially for plug-in hybrid electric vehicles (PHEVs). Although significant progress has been made during the last 20 years in various battery systems, existing systems do not satisfy all of the energy-storage needs for PHEV applications. More improvements are needed with respect to energy density, power density, cycle life, safety, and cost of lithium-ion batteries. Commercial lithium batteries primarily use graphite-based anodes, which have a specific capacity of 372 mAh g^{-1} (LiC_6). Alternative anodes based on lithium–metal alloys have been actively pursued in recent years. Among these lithium–metal alloys, an alloy with silicon ($Li_{21}Si_5$) has the highest theoretical specific capacity of nearly 4200 mAh g^{-1}. However, very large volume changes (more than 300 percent increase in volume) occur when the lithium and graphite are alloyed. This large volume change can cause severe cracking and pulverization of the electrode, and lead to significant capacity loss. Many efforts have been made to mitigate this problem [1–4]. Chan et al. [5] reported silicon nanowires (diameter < 100 nm) prepared using a CVD method based on vapor–liquid–solid (VLS) mechanism that used silane gas as the silicon source. During the initial lithium insertion, these nanowires were capable of charging up to the theoretical capacity without pulverization, which is a common phenomenon observed in bulk, micro-, and even nano-particulate silicon. After transforming into amorphous Li_xSi, the one-dimensional nano-silicon maintained a charge capacity of 75 percent of its theoretical capacity, with little fading during cycling. Also, the shortened lithium transport in the silicon nanostructure and the low-resistance electrical connection led to an excellent rate capability (>2100 mAh g^{-1} at 1 C). Yu et al. [6] employed an alternative approach in which silicon-based nanowires were prepared on solid silicon wafers using the solid–liquid–solid (SLS) mechanism. In this approach, the solid silicon wafers acted as the silicon source. In both of the approaches described above, silicon nanowires were grown on the surface of solid substrates (i.e., stainless steel or silicon wafers) that are usually much thicker and heavier than the nanowires themselves. While sufficient for concept demonstration and material design, significant work still needs to be done to improve the practical specific capacity of such anodes (including the substrate and current collector) before they can be used in large-scale applications.

Several other approaches have been used to grow silicon-based nanowires [7–10]. For example, Kolb et al. [9] prepared silicon-based nanowires by evaporating silicon monoxide (SiO) in an inert gas atmosphere using a gold-coated silicon wafer as a substrate. Chang et al. [10] reported growth of silicon-based nanowires by heat treatment of an iron-catalyst coated silicon nanopowder at

* Corresponding author. Tel.: +1 509 372 6515; fax: +1 509 375 3864.
E-mail address: jiguang.zhang@pnl.gov (J.-G. Zhang).

0378-7753/$ – see front matter. Published by Elsevier B.V.
doi:10.1016/j.jpowsour.2009.09.068

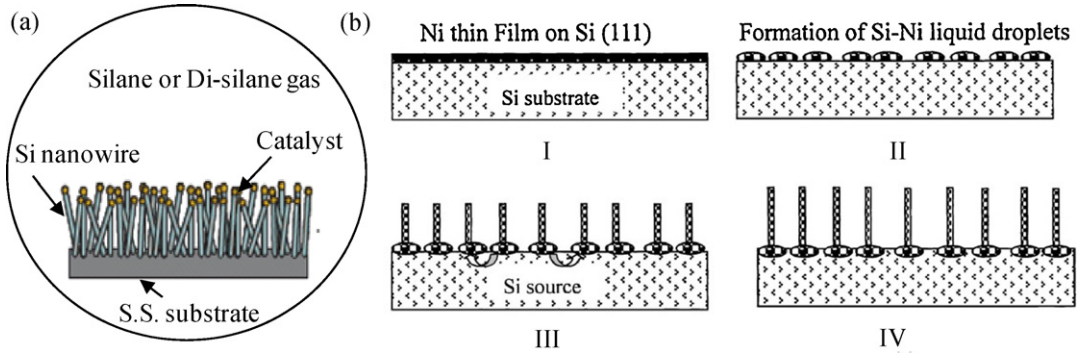

Fig. 1. Two-dimensional growth of Si nanowires. (a) Grown on stainless steel substrate via VLS process [5]; (b) grown on silicon wafer via SLS process [6].

980 °C. However, no electrochemical performances of these silicon-based nanowires were reported.

In this work, free-standing silicon-based nanowires were prepared from commercial silicon powders in a three-dimensional manner rather than on the surface of the substrate (i.e., two-dimensional growth). The vapor-induced solid–liquid–solid (VI-SLS) mechanism is proposed to explain the growth of multicomponent nanowires from solid powder sources. The composition, morphology, crystal structure, and the electrochemical performance of the nanowires were investigated.

2. Experimental

Although many literatures (see Refs. [6–11]) have reported preparation of "silicon nanowires," we notice that most nanowires reported in the previous works include not only Si, but also SiO_x, SiC or other impurities, especially for nanowires grown at a temperature of more than 800 °C. To avoid confusion, we will use the term "silicon-based nanowires" to represent the nanowires grown in this work before their specific compositions are determined. Fig. 1 shows the schematic of silicon-based nanowire grown on a two-dimensional surface by (a) the VLS process [5] and (b) the SLS process [6]. In this case, wire growth is unidirectional and perpendicular to the substrate surface. Fig. 2 shows the schematic of silicon-based nanowires grown from silicon powders contained in the whole volume of the container (three-dimensional growth) instead of only on the surface of the container (two-dimensional growth). In this case, nanowire growth is radial, as shown in Fig. 2. A description of the steps involved in growing silicon-based nanowires using the VI-SLS process follows: etched silicon powders (1) are coated with nickel-based catalysts (2). Silicon-based nanowires (3) grown from individual silicon powders through the VI-SLS mechanism and silicon powders are consumed. Finally, long silicon-based nanowires (4) are obtained after silicon powders are mostly consumed. No expensive or toxic precursors have been used in this approach. The three-dimensional growth also means that this process can be more easily adapted to large-scale production relative to two-dimensional growth approaches.

Two furnaces have been used to grow silicon-based nanowires. Furnace #1 is a high-temperature furnace (Model 1000-45120-FP30, Thermal Technology, Inc.) with a graphite liner as shown in Fig. 3. An optional oxygen trap (Alletech High-Pressure Oxy-Trap, Part No. 8115) is used in the gas line to remove residual oxygen. After purification, the gas stream should contain less than 1 ppb O_2. Furnace #2 is a quartz tube furnace (Lindberg Hevi-Duty 54291-A) as shown in Fig. 4. Various gases with or without oxygen are introduced into the furnace to assist on the nanowire growth. Silicon powders (325 mesh) received from Sigma–Aldrich were ground in a high-energy milling system (SPEX 8000M) using a stainless steel vial for 5 h. The samples have an average particle size of ~0.1 μm after milling. The ground sample was etched with dilute hydrofluoric acid (HF) and then was coated with 10 percent nitrogen using an aqueous $Ni(NO_3)$ solution. The dried powder was placed in a ceramic boat and positioned in the center of the furnace. The furnace was pumped down to 10^{-3} Torr and refilled with an argon/hydrogen mixture (2.75 percent hydrogen). This process was repeated three times to minimize the residual air in the furnace. The furnace then was filled with an argon/hydrogen mixture, and the pressure in the furnace was controlled between 50 and 200 Torr by adjusting the gas flow rate and pumping speed. The furnace initially was heated at a rate of 5 °C min^{-1} to 500 °C and then held there for 1 h. After one hour, the furnace was heated at

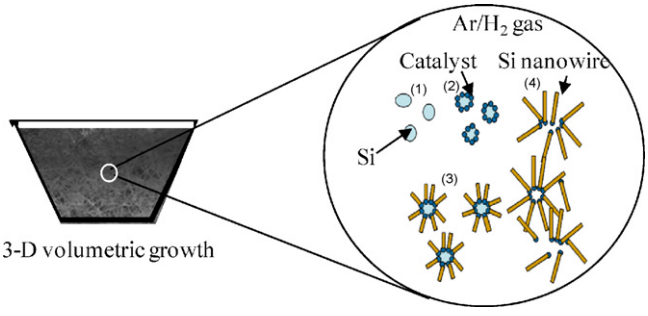

Fig. 2. Schematic of three-dimension grow of silicon-based powders from Si powder in VI-SLS method. (1) Etched silicon powders; (2) nickel catalysts coated silicon powders. (3) Silicon nanowires grown from individual silicon particles through the VI-SLS mechanism. (4) Grown silicon nanowires after silicon powders are largely consumed.

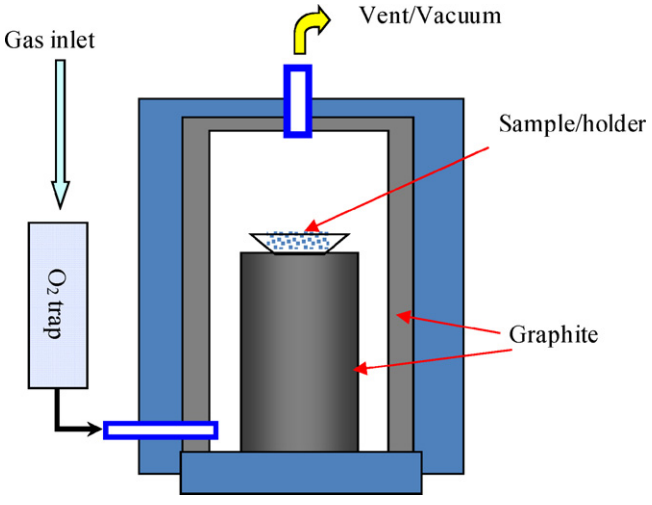

Fig. 3. High temperature vacuum furnace with a graphite liner.

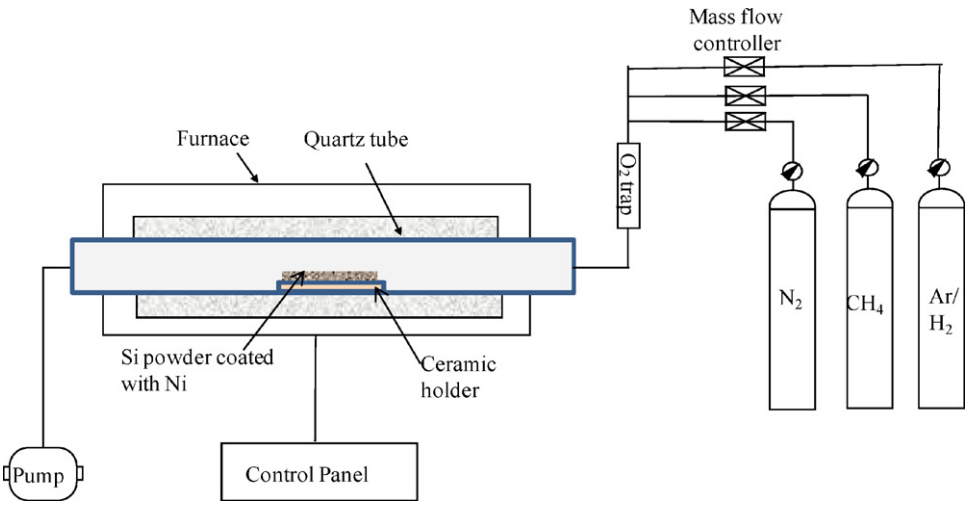

Fig. 4. Schematic of a furnace with quartz tube used for nanowire growth.

a rate of 10 °C min^{-1} to 950 °C and then held there for 2–6 h. After silicon-based nanowire growth, the samples were cooled to room temperature at a rate of 10 °C min^{-1}.

The morphologies of silicon precursors and nanowires have been analyzed by scanning electron microscopy (SEM) (JEOL JSM-5900LV). The crystal structures of precursors and nanowires have been analyzed by X-ray diffraction spectroscopy in Θ to 2Θ scan mode using a Philips Xpert X-ray diffractometer using copper Kα radiation at $\lambda = 1.54$ Å. Both the morphology and the crystal structure also were investigated by transmission electron microscopy (TEM) (JEOL JEM 2010, operated at 200 kV) and energy dispersive X-ray spectroscopy (EDX) (Oxford Link system). Electrochemical tests of the silicon-based anode were performed on coin cells (type CR2325) assembled in an argon-filled glove box. The silicon-based nanowires were mixed with carbon black (Super P, 40 nm, Timcal) and CMC binder (sodium carboxymethyl cellulose, Sigma–Aldrich) at a ratio of 80:12:8 in water. The slurry was cast on copper foil as an anode and dried at 90 °C in air overnight to remove water. Electrodes that were 1.27 cm in diameter were punched from the coated copper foil and used as the working electrode. Lithium foil was used as the counter electrode. A microporous polypropylene membrane (Celgard 2502) was used as a separator and 1 M $LiPF_6$

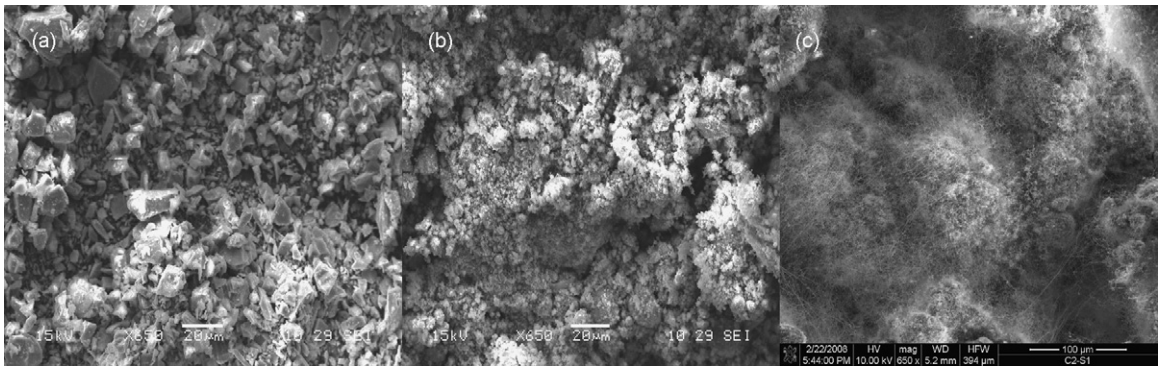

Fig. 5. SEM micrograph of silicon powders before and after nanowire growth in a furnace with graphite liner. (a) As received silicon powder. (b) Silicon powder after ball milling for five hours. (c) Silicon nanowires grown from silicon powder.

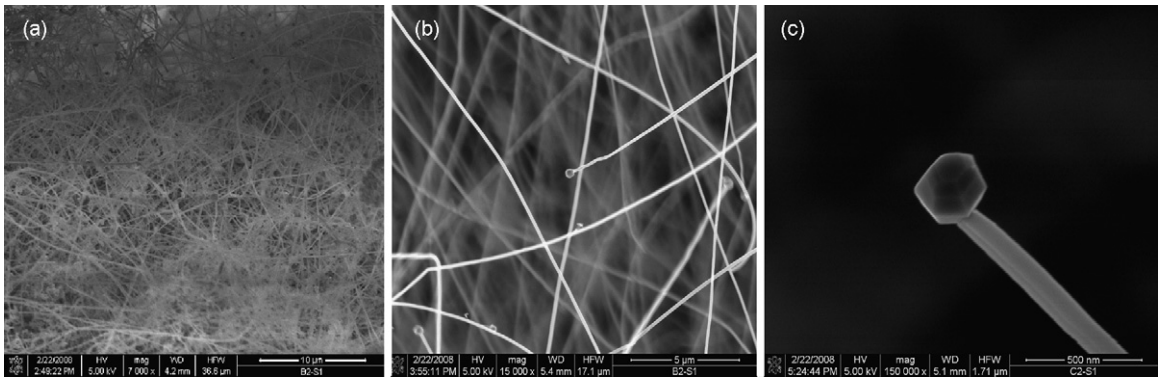

Fig. 6. SEM micrograph of SiNWs grown in a furnace with graphite liner. (a) Low resolution micrograph of nanowire. (b) Mid resolution micrograph of nanowires. (c) High resolution micrograph of nanowires with the crystalline tip.

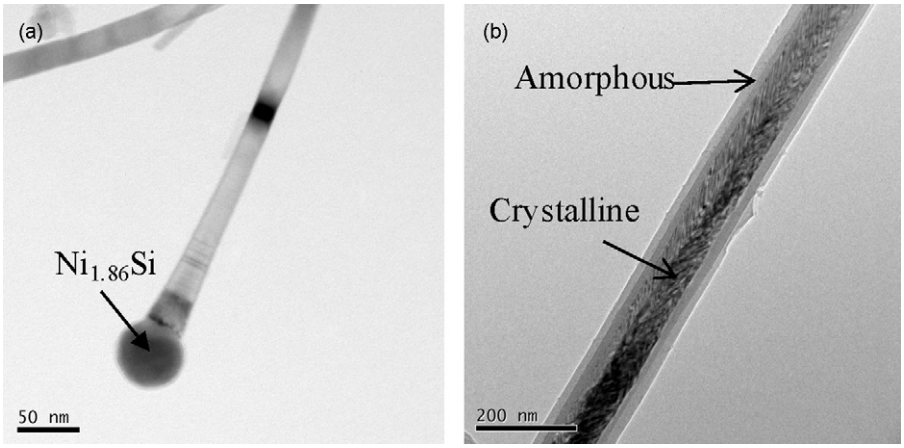

Fig. 7. TEM micrograph of SiNWs grown in a furnace with graphite liner. (a) Micrograph of the tip of nanowires. EDX analysis revealed that the composition of the tip is $Ni_{1.86}Si$. The nickel is from catalyst coated on the surface of silicon powders. (b) Detail of nanowire with a crystalline core and amorphous shell.

in an ethylene carbonate/diethyl carbonate (EC/DEC) 1:2 mixture was used as the electrolyte.

3. Results and discussion

Fig. 5 shows SEM micrographs of silicon powders before and after nanowire growth in a furnace with a graphite liner. As-received silicon powder has a particle size of 5–20 μm (see Fig. 5(a)). The particle size was reduced to ~0.1–1 μm by processing a ball mill for five hours (see Fig. 5(b)). Fig. 5(c) shows that silicon-based nanowires grown from silicon powders resided throughout the containers rather than just on the surface. More details of the nanowires are shown in Fig. 6. Fig. 6(a) shows a low-magnification micrograph of silicon-based nanowires, while Fig. 6(b) is a high-magnification image of nanowires where multiple nanowires with tips are clearly visible. Fig. 6(c) reveals details of the nanowires with a crystalline tip. Fig. 7 shows a TEM micrograph of silicon-based nanowires grown in a furnace with a graphite liner. EDX analysis (see Fig. 7(a)) revealed that the composition of the tip is $Ni_{1.86}Si$. The nickel originated from catalyst that was coated on the surface of the silicon powders. Fig. 7(b) shows that the nanowire grown in the furnace with graphite liner has a crystalline core and an amorphous shell. From a comparison of the results of the selected area electron diffraction (SAED) analysis of the crystalline core in the nanowires (see Fig. 8) with those of the standard diffraction pattern shown in Table 1, it is clear that the crystal core of the nanowire was dominated by SiC. The crystal structure of the silicon precursors and nanowires were further analyzed by X-ray diffraction. Fig. 9(a) shows the X-ray spectra of the HF-etched silicon precursor before nanowire growth. No SiC peaks were observed. Fig. 9(b) shows the X-ray spectra of silicon-based nanowires grown in the furnace with a graphite liner. SiC peaks were clearly identified in silicon-based nanowires. We note that the EBSD pattern shown in Fig. 8 reveals that the localized core structure of a single nanowire consists of

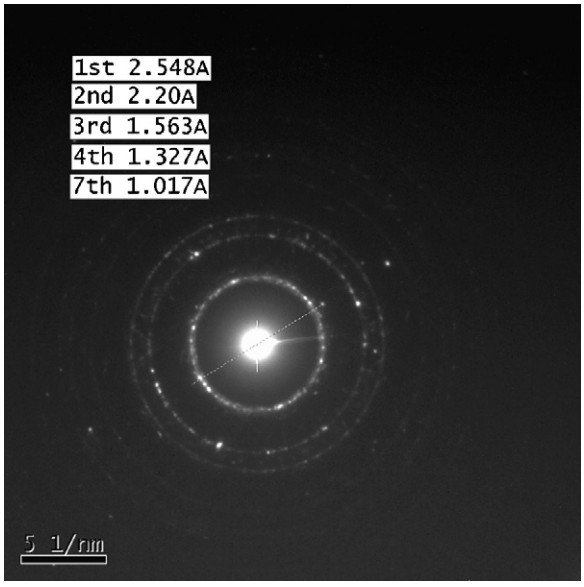

Fig. 8. The selected area electron diffraction (SAED) of the crystalline core in the nanowires is consistent with cubic structured 3c–SiC.

almost pure SiC. However, the X-ray diffraction pattern shown in Fig. 9(b) shows the collective pattern of a large amount of silicon-based nanowires. The later spectrum includes the contribution from both SiC cores of nanowire and un-reacted silicon powders.

The combination of EDX and SAED analysis also shows that the shell of nanowire shown in Fig. 7(b) is amorphous silicon oxide. Formation of nanowires (grown in the furnace with a graphite liner) with a crystalline SiC core and a SiO_x shell can be explained as the following. When silicon-based nanowires grown in a furnace with a graphite liner, residual oxygen in the carrier gas will react

Table 1
X-ray diffraction pattern of Si and SiC.

Silicon, Fd3m, a = 5.43088 Å					SiC (Moissanite-3C), F-43m, a = 4.3589 Å				
#	d (Å)	2θ	($h\,k\,l$)	I (f)	#	d (Å)	2θ	($h\,k\,l$)	I (f)
1	3.1355	28.442	(1 1 1)	100	1	2.5200	35.597	(1 1 1)	100.0
2	1.9201	47.302	(2 2 0)	55.0	2	2.180	41.383	(2 0 0)	20.0
3	1.6375	56.121	(3 1 1)	30.0	3	1.5411	59.977	(2 2 0)	35.0
4	1.3577	69.130	(4 0 0)	6.0	4	1.3140	71.777	(3 1 1)	25.0
5	1.2459	76.377	(3 3 1)	11.0	5	1.2583	75.492	(2 2 2)	5.0

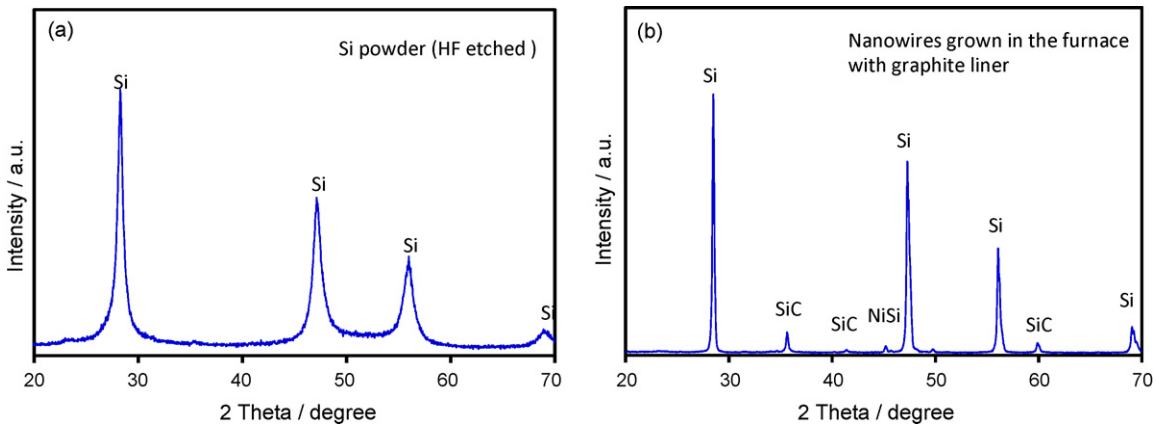

Fig. 9. X-ray diffraction pattern of (a) HF etched silicon powder before nanowire growth and (b) nanowires grown in the furnace with graphite liner.

with carbon to form CO, the CO then will react with silicon in the nickel–silicon alloy and form a SiC core (which will condense first because it has a melting point (2730 °C) much higher than those of SiO_2 (1710 °C)). The oxygen remaining from the above reaction described above will combine with silicon to form a SiO_x shell outside a SiC core. The temperature in this shell is lower than that in the center of nanowires. The disproportionation reaction can be expressed as:

$$CO + Si\,(\text{in Ni–Si alloy}) \overset{950\,^{\circ}C}{\longrightarrow} SiC + SiO_x \quad (1)$$

This process is responsible for the nucleation of SiC on the surface of silicon particles. For further growth of nanowires, gas phased SiO may play an important role and can be expressed as:

$$CO + SiO(g)\,(\text{in Ni–Si alloy}) \overset{950\,^{\circ}C}{\longrightarrow} SiC + SiO_x \quad (1')$$

Simultaneous formation of SiC and SiO_x leads to faster growth of nanowires in a graphite-lined furnace when compared with the growth of only SiO_x in a furnace without a graphite liner operated under the similar conditions (which will be discussed later). The thickness ratio of the SiC core to the SiO_x shell depends on the amount of oxygen available and the formation possibility of the SiC and the SiO_x under the given conditions (i.e., the temperature and the ratio of the residual gases). Therefore, it is possible to control the thickness ratio of SiC core and SiO_x shell by controlling the amount of residual oxygen and CO in the processing gas. Fig. 10(a) shows a TEM micrograph of silicon-based nanowires grown in a graphite-lined furnace with no oxygen trap. A thick amorphous SiO_x layer can be seen in the figure. After an oxygen trap was installed, the thickness of the SiO_x layer decreased significantly, and the nanowires were dominated by a SiC core as shown in Fig. 10(b).

To eliminate the formation of SiC in the nanowires, the silicon-based nanowires were prepared in a furnace equipped with a quartz tube but no graphite liner (see Fig. 4). In this case, all of the preparation parameters (e.g., sample etching, nickel coating, heat treatment, etc.) were the same as described in the previous sections. Fig. 11 shows a TEM micrograph and EBSD of a silicon-based nanowire grown in the quartz tube, which is carbon-free. From the TEM micrograph, it is apparent that the nanowire has a uniform structure with no crystalline core, while the EBSD pattern indicated that the nanowire is amorphous. The composition of the nanowire is predominately $SiO_{1.8}$ as measured by energy dispersive spectroscopy. By combining these analyses with X-ray photoelectron spectroscopy of the surface of nanowire, these nanowires were identified as amorphous SiO_x where x ranges from 1.7 to 1.88. Several procedures have been adopted to reduce the oxygen content in the nanowires. However, the growth rate of the nanowires was reduced significantly after these procedures were adopted. When residual oxygen was present, either incidental or intentional, SiO_x nanowires were observed. In a separate experiment, a thin layer (~50 nm) of nickel was sputter coated on a silicon substrate and placed in quartz furnace as a reference sample. The nickel–silicon surface was half exposed and half covered. The nanowire growth rate was significantly reduced in the covered portion of nickel-coated silicon substrate. This observation indicates that the gas component is necessary for nanowire growth.

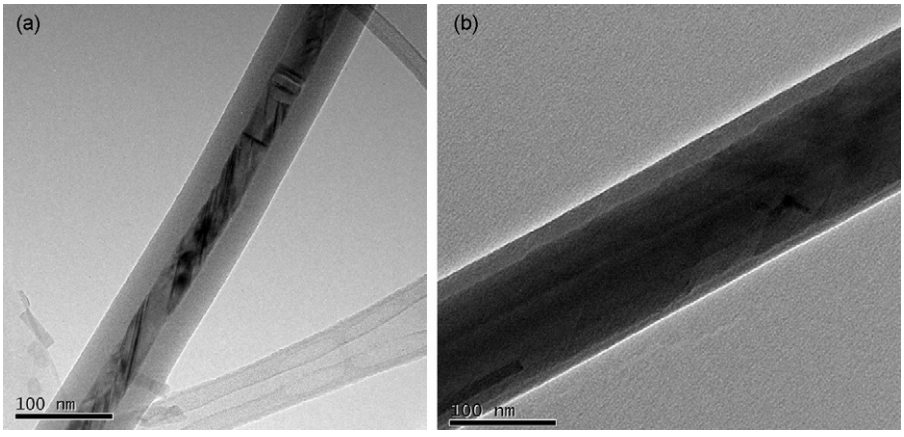

Fig. 10. TEM micrograph of silicon-based nanowires. (a) Micrograph of nanowires grown in graphite furnace with no O_2 trap. (b) Micrograph of nanowires grown in graphite furnace after O_2 trap was installed.

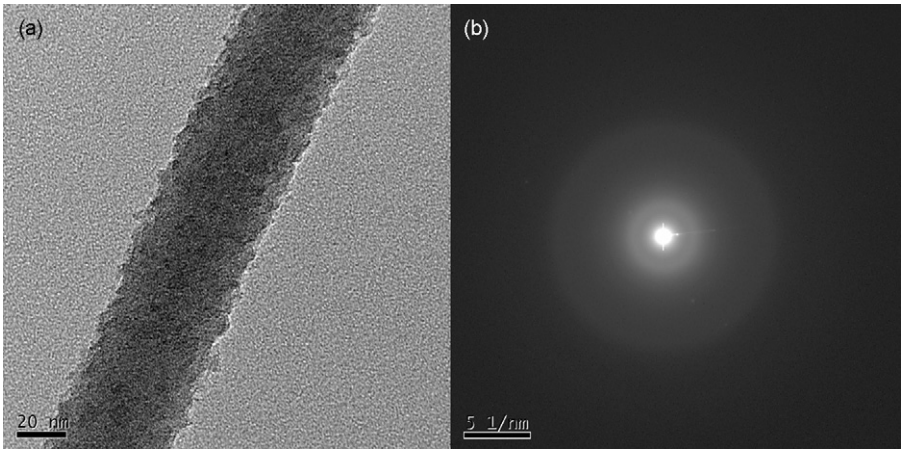

Fig. 11. (a) TEM micrograph and (b) electron diffraction pattern of SiNWs prepares in a carbon free furnace with no oxygen trap. EDX analysis revealed that the composition of the nanowire is $\sim SiO_{1.8}$.

The nanowire growth process can be expressed as follows:

$$O_2(g) + Si\,(\text{in Ni–Si alloy}) \xrightarrow{950\,^{\circ}C} SiO_x(s) \rightarrow SiO_x \text{ nanowire} \quad (2)$$

Oxygen in the process may come from two sources: from the unetched SiO_x layer left on the surface of silicon particles or oxygen residual in the precursor gases. Yang et al. [11] calculated the equilibrium oxygen partial pressure with respect to formation of CO and SiO. Their results indicate that only very low equilibrium oxygen partial pressures (about 10^{-10} Pa at 1600 °C) are required to form CO and SiO. This pressure is less than the oxygen impurity in pure argon used in our experiment. We also noticed that the growth rate of nanowires was significantly reduced after an oxygen filter was installed on the precursor gas line. This result clearly demonstrates that the majority of oxygen for reaction (2) is from the oxygen impurity in precursor gases.

The electrochemical properties of silicon-based nanowires (with a typical composition of $SiO_{1.8}$) grown in a quartz furnace were investigated. Fig. 12 shows the charge/discharge profile and specific capacity of $SiO_{1.8}$ nanowires during the first two cycles. The sample was discharged at a rate of *C*/20 between 0.02 and 1.5 V. The sample shows an initial charge capacity of 1800 mAh g^{-1} and a discharge capacity of ~1300 mAh g^{-1}. The relatively large first cycle loss can be attributed to the formation of solid electrolyte interface layers. The initial discharge capacity of 1800 mAh g^{-1} is smaller than the theoretical specific capacities of $Li_{21}Si_5$ (4200 mAh g^{-1}), but it is larger than those of SiO reported in literature [12]. The discharge/charge capacities mainly come from lithium intercalation/extraction in SiO_x shell and may also partially come from lithium intercalation/extraction in Si core. This is consistent with the observation that the nanowires prepared in this work were a mixture of Si core and SiO_x shell.

Based on a mechanism proposed by Yu et al. [6], the driving force for nanowire growth in SLS process is the temperature difference between the substrate and the outside surface of the Ni_xSi alloy. However, this mechanism cannot be used to explain nanowire growth in silicon powders. In this case, the particle size is so small that the temperature difference between inside and outside of sample is not enough for silicon-based nanowires to grow. We suggest that the VI-SLS mechanism be used to explain nanowire growth in silicon powders. The VI-SLS process needs both vapor and solid precursors for nanowire growth. It can be understood as a combination of the VLS process (where the nanowire is grown from gas source) and the SLS process (where the nanowire is grown from solid source). It requires the presence of both gas and solid sources. The gas precursor can be oxygen-, nitrogen-, carbon-, or silicon-containing gases. In this mechanism, the vapor source will first combine with silicon in the nickel–silicon alloy to form nanowires, and then more silicon from silicon powders will be dissolved in the silicon-deficient nickel–silicon alloy. This process will continue until either the gas source or the solid source is exhausted. This mechanism not only explains our experimental results, but also can be used to guide the design and preparation of non-silicon-based

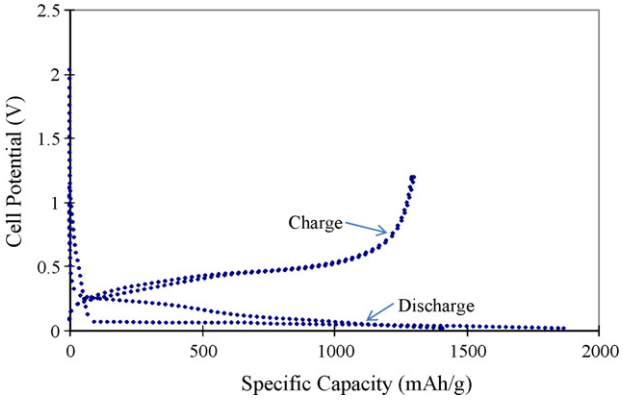

Fig. 12. Charge/discharge properties of SiNWs grown from silicon powder. The samples demonstrate a discharge capacity of ~1300 mAh g^{-1}.

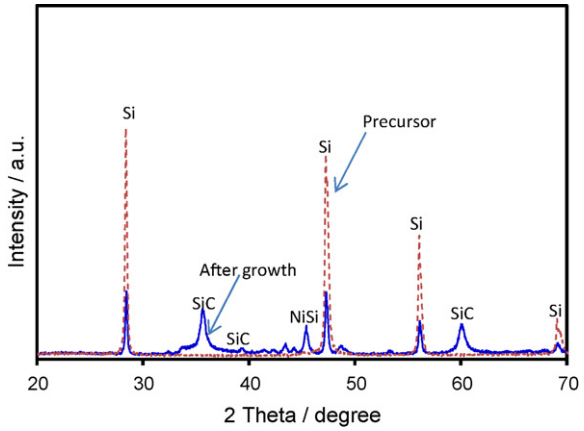

Fig. 13. X-ray diffraction pattern of silicon precursor and nanowires grown in a quartz furnace with intentional introduction of carbon source (CH_4). SiC is clearly identified in the nanowires.

nanowires, using materials such as Ge, Ge_3N_4. GeO, GeO_2, Sn, SnO, or SnO_2.

To verify the proposed VI-SLS mechanism, an experiment has been designed to prepare SiC nanowires in a carbon-free furnace (in a quartz tube) using silicon powder as the silicon source and CH_4 gas as an intentional carbon source. In this case, all of the preparation parameters (the sample etching, nickel coating, heat treatment, etc.) were the same as described in the previous sections except that 1 percent CH_4 gas was introduced into the operating gas (argon/2.75 percent hydrogen). Fig. 13 shows the X-ray diffraction pattern of the silicon precursor and the nanowires grown in a quartz furnace with intentional introduction of a carbon source (CH_4). The X-ray pattern of the original precursors shows only peaks associated with crystalline silicon. However, SiC peaks were clearly identified in the nanowires grown in quartz furnace with the intentionally introduced carbon source. The nanowire growth process can be expressed as follows:

$$CH_4(g) + Si\,(\text{in Ni–Si alloy}) \xrightarrow{950\,^{\circ}C} SiC(s) + H_2 \uparrow \rightarrow \text{SiC nanowire} \qquad (3)$$

4. Conclusion

Silicon-based nanowires have been grown from catalyst-coated silicon powders under different oxygen and carbon activities. Nanowires grown in the presence of carbon sources consist of a crystalline SiC core and an amorphous SiO_x shell. The thickness of the SiO_x shell decreases with lowered oxygen concentration in the precursor gases. Nanowires grown in the carbon-free environment consisted of amorphous silicon oxide with a typical composition of $SiO_{1.8}$. The growth rate of nanowires also decreases with decreasing oxygen content in the precursor gases. $SiO_{1.8}$ nanowires exhibit an initial discharge capacity of $\sim$1300 mAh g^{-1}, but their capacity retantion still needs to be improved for practical application. We believe that the VI-SLS mechanism explains nanowire growth from powder sources, especially the growth of silicon-based nanowires. In this approach, both the gas source (such as oxygen-, nitrogen-, carbon-, or silicon-containing gases, etc.) and the solid source (in powder form) are used for nanowire growth under the given conditions. The VI-SLS mechanism requires the presence of both gas and solid sources. This mechanism can be seen as a combination of the VLS process (where only a gas source was used to grow the nanowire) and the SLS process (where only the solid source was used to grow the nanowire). This mechanism can explain all of our experimental results. It can also used to guide the design and preparation of other nanowires.

Acknowledgements

The authors thank Laxmikant V. Saraf and James E. Coleman for their help with the SEM analysis. This work is supported by the Laboratory Directed Research and Development (LDRD) Program of Pacific Northwest National Laboratory and by the Department of Energy through the Office of Vehicle Technology. Part of the research was performed in the Environmental Molecular Sciences Laboratory, a national scientific user facility sponsored by DOE's Office of Biological and Environmental Research and located at PNNL.

References

[1] Moni Kanchan Datta, Prashant N. Kumta, J. Power Sources 158 (2006) 557–563.
[2] http://www.sandia.gov/news-center/news-releases/2003/renew-energy-batt/betterlithium.html.
[3] Si Hyoung Oh, Young Hwan Jung, Hyung Sun Kim, Kyung Yoon Chung, Dong Jin Byun, Byung, Won Cho, Abstract 169, 211th Electrochemical Society Meeting, May 6–10, 2007, Chicago.
[4] Ikuo Yonezu, Hisaki Tarui, Seiji Yoshimura, Shin Fujitani, and Toshiyuki Nohm, SANYO Electric Co., Ltd., Abs. 58, IMLB 12 Meeting, © 2004 The Electrochemical Society, Inc.
[5] Candace K. Chan, Hailin Peng, Gao Liu, Kevin McIlwrath, Xiao Feng Zhang, Robert A. Huggins, Yi Cui, Nat. Nanotechnol. 3 (2008) 31–35.
[6] D.P. Yu, Y.J. Xing, Q.L. Hang, H.F.Y. Saraf, Laxmikant Van, J. Xu, Z.H. Xi, S.Q. Feng, Physica E 9 (2001) 305–309.
[7] S.M. Prokes, Stephen Arnold, Appl. Phys. Lett. 86 (2005) 193105.
[8] R.-Q. Zhang, Y. Lifshitz, S.-T. Lee, Adv. Mater. 15 (2003) 635.
[9] F.M. Kolb, H. Hofmeister, R. Scholz, M. Zacharias, U. Gosele, D.D. Ma, S.-T. Lee, J. Electrochem. Soc. 151 (2004) 472–475.
[10] J.B. Chang, J.Z. Liu, P.X. Yan, L.F. Bai, Z.J. Yan, X.M. Yuan, Q. Yang, Mater. Lett. 60 (2006) 2125–2128.
[11] Guangyi Yang, Renbing Wu, Jianjun Chen, Yi Pan, Rui Zhai, Lingling Wu, Jing Lin, Nanotechnology 18 (2007) 155601.
[12] T. Zhang, J. Gao, H.P. Zhang, L.C. Yang, Y.P. Wu, H.Q. Wu, Electrochem. Commun. 9 (2007) 886–890.